IPP-Report

IPP Max-Planck-Institut für Plasmaphysik

C.D. Beidler, E. Harmeyer, F. Herrnegger, Yu. Igitkhanov,
A. Kendl, J. Kisslinger, Ya.I. Kolesnichenko,
V.V. Lutsenko, C. Nührenberg, I. Sidorenko,
E. Strumberger, H. Wobig, Yu.V. Yakovenko

The Helias Reactor HRS4/18

IPP III/268

Februar 2001

The Helias Reactor HSR4/18

C.D. Beidler, E. Harmeyer, F. Herrnegger, Yu. Igitkhanov, A. Kendl, J. Kisslinger, Ya.I. Kolesnichenko[1], V.V. Lutsenko[1], C. Nührenberg, I. Sidorenko, E. Strumberger, H. Wobig, Yu.V. Yakovenko[1]

Max-Planck Institut für Plasmaphysik, EURATOM Association D-85740 Garching bei München, Germany.
[1] Scientific Centre "Institute for Nuclear Reseach" 03680 Kyiv, Ukraine

Abstract: The Helias reactor is a scaled-up version of the Wendelstein 7-X experiment. A straightforward extrapolation of Wendelstein 7-X leads to HSR5/22, which has 5 field periods and a major radius of 22 m. HSR4/18 is a more compact Helias reactor with 4 field periods and 18 m major radius. Stability limit and energy confinement times are nearly the same as in HSR5/22, thus the same fusion power (3000 MW) is expected in both configurations. Neoclassical transport in HSR4/18 is very low; the effective helical ripple is below 1%. This paper describes the power balance of the Helias reactor, the blanket and maintenance concept. The coil system of HSR4/18 is comprised of 40 modular coils with NbTi-superconducting cables. The reduction from 5 to 4 field periods and the concomitant reduction in size will also reduce the cost of the Helias reactor.

1. Introduction

The Wendelstein 7-X experiment, which is under construction in the city of Greifswald, is the basis of the current Helias reactor studies. HSR5/22 (5 field periods, major radius 22 m) is a straightforward extrapolation of Wendelstein 7-X [1]. In order to reduce the size of the reactor another option with 4 field periods and a major radius of 18 m has been investigated and the results obtained are the subject of this paper. The main optimisation principle of the Helias reactor is the reduction of the Pfirsch-Schlüter currents and the Shafranov shift while maintaining a MHD-stability limit of $<\beta>$ above 4%. A further important goal is to eliminate prompt α-particle losses as much as possible and to provide confinement of trapped α-particles for one slowing down time. The modular coil system comprises 10 coils per period, which are constructed using NbTi-super-conducting cables. This implies that the maximum magnetic field on the coils must not exceed 10 T. The data of the present and past Helias reactors are listed in the following table.

TABLE I: Main parameters of HSR4/18 and HSR5/22

		HSR4/18	HSR5/22
Major radius	[m]	18	22
Average minor radius	[m]	2.0	1.8
Plasma volume	[m^3]	1420	1407
Iota(0)		0.83	0.84
Iota(a)		0.96	1.00
Average magnetic field on axis	[T]	5.0	5.0
Maximum magnetic field on coils	[T]	10	10.3
Number of coils		40	50
Magnetic energy	[GJ]	80	100

2. Coil System of the Helias Reactor

The coil system of the Helias reactor HSR5/22 consists of 50 modular coils. There are 10 coils in every period, however, only 5 different types of coils exist due to the symmetry of the magnetic field and the coil system. In HSR4/18 the number of coils is 40, and again there are 10 coils per period. The shape of the coils is essentially the same as in the 5-period reactor. Less than 10 coils per period would facilitate accessibility to the blanket, but this also would raise the modular ripple and the losses of highly energetic alpha particles. By shaping the winding pack into a trapezoidal form the maximum magnetic field on the coils can be reduced to 10 T, while the averaged magnetic field on axis is nearly 5 T. The trapezoidal shape reduces the current density in the high field region in the coil. There is a sufficient safety margin with regards to the maximum field limit of a NbTi-superconductor [2], if forced flow cooling with super-critical Helium at 1.8 K is applied [3].

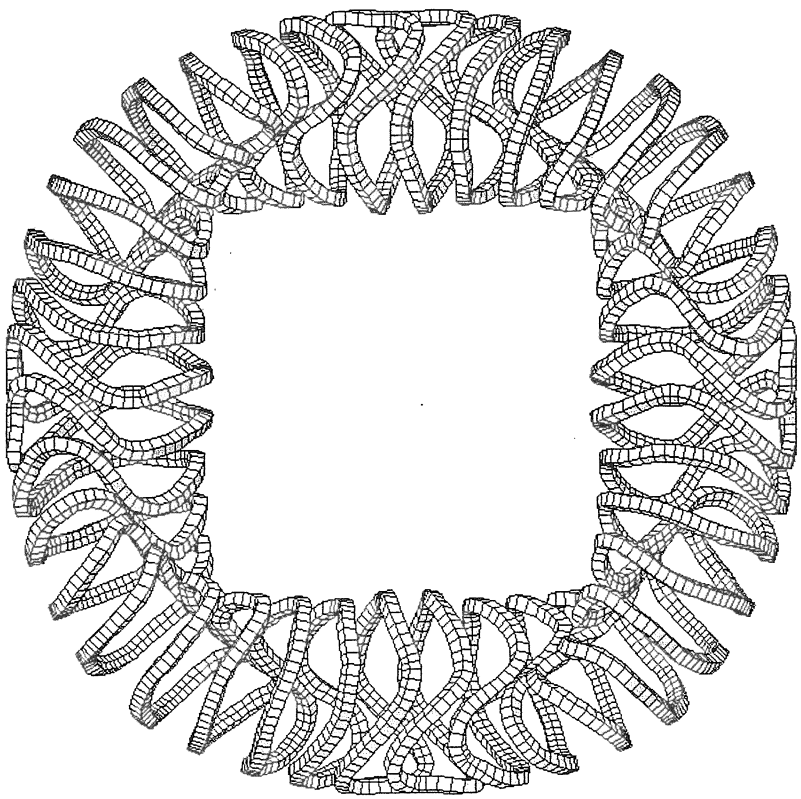

FIG. 1: HSR4/18, Top view onto the coil system depicting winding pack plus casing; the coil support system is not shown.

The mechanical stresses in the coils strongly depend on the geometry of the support system. This support system consists of the coil casing and the intercoil support elements, which are not shown in Fig. 1. In designing this support system a compromise could be reached between the need to minimize the stresses and the desire for optimum access to blanket and the plasma chamber. Stress analysis of the coil system in HSR5/22 has been performed using the ANSYS code [4].In these computations the orthotropic elastic data of the envisaged "cable in conduit" were used in the winding pack, while for coil housing and intercoil structure the elastic data of stainless steel with E = 210 GPa, ν =0.3 and a non-linear stress-strain curve with a yield stress of 800 MPa were applied. The maximum stress found in the coil housing is 650 MPa

leading to a maximum displacement of 35 mm. Locally the deformation is larger than 0.2%, which implies that further optimisation of the support system is needed to reduce the local stress maxima.

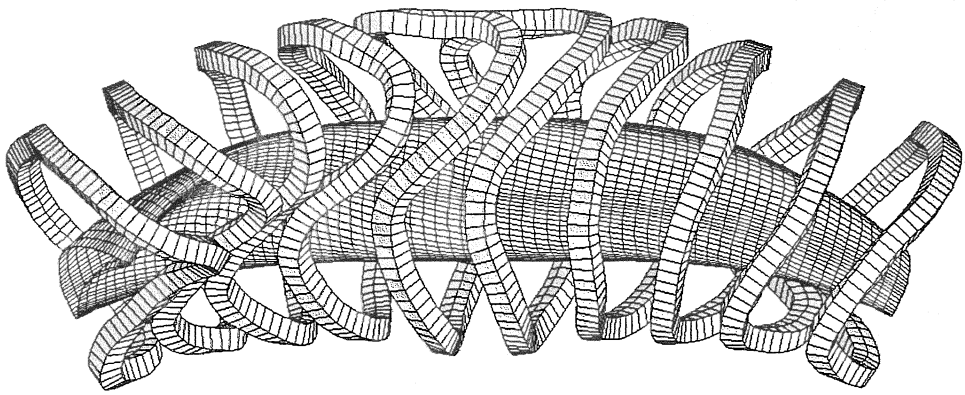

FIG. 2: *One period of the coil system and plasma, top view.Numbering of coils from left to right: 1,2, ..10. There are only 5 coils with different shape*

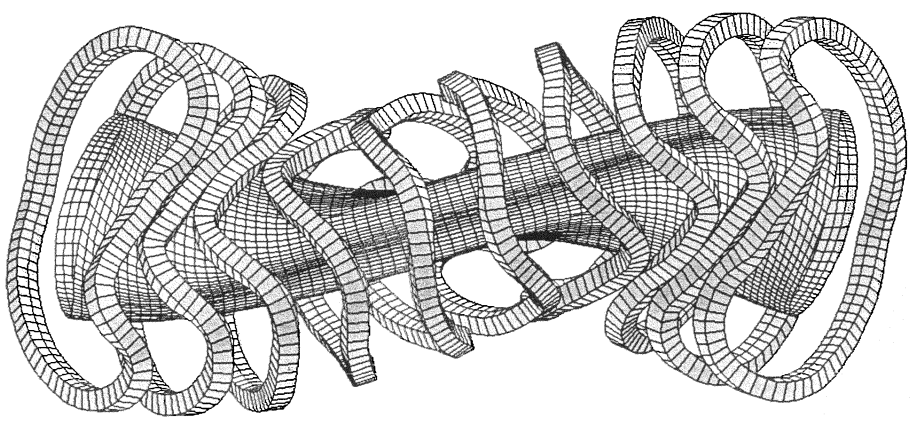

FIG. 3: *One period of the coil system and plasma, horizontal view from inside*

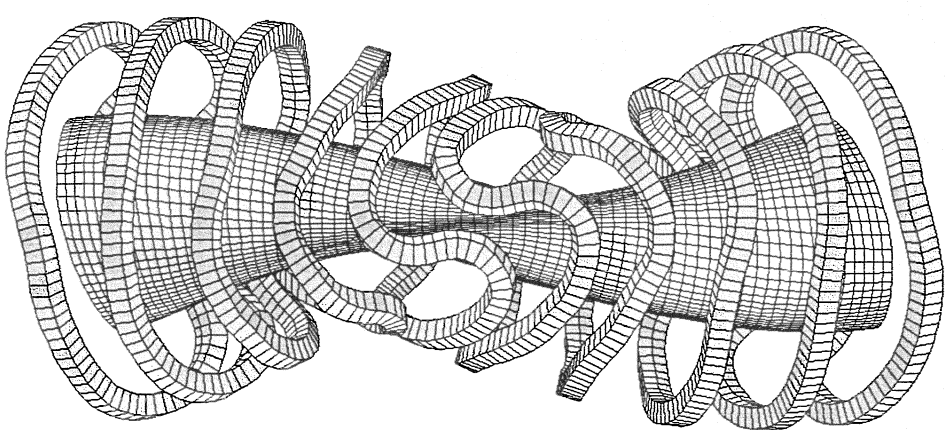

FIG. 4: *One period of the coil system and plasma, horizontal view from outside*

In contrast to the Wendelstein 7-X experiment no auxilliary coils are needed, since the magnetic field need not be varied under reactor conditions.

1.1. The conductor

A 'cable-in-conduit' conductor has been proposed by FZK (W. Maurer) using NbTi at 1.8 K with forced-flow cooling of superfluid helium. This conductor is an upgraded version of the conductor used in Wendelstein 7-X. The maximum current will be 40 kA. The dimensions of the cross-section without insulation are 32x32 mm, and the bore for the SC-cable and the He is 22 mm. For the proposed 40 kA conductor, 192 strands of pure copper and NbTi-filaments are cabled together in order to keep AC losses sufficiently low.

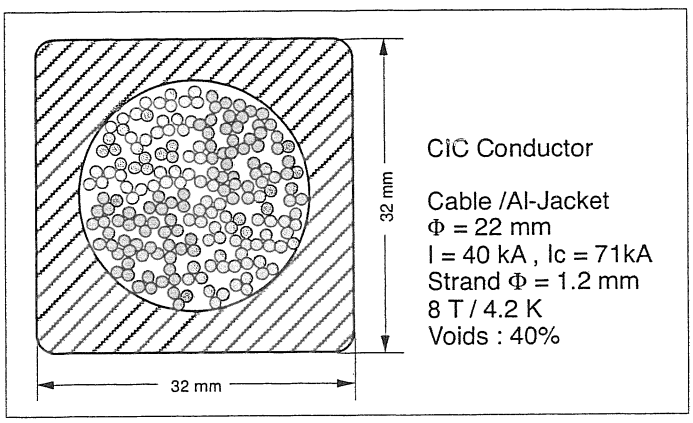

FIG. 5: *Proposed SC cable for HSR 4/18*

Table 1: *Main data of the super conductor*

Al-Jacket		
Width	[mm]	32
Height	[mm]	32
Bore [mm]		22
Specific weight [t/m^3] (Al)		2.7
Weight	[kg/m]	1.73
Cable (Void [40 %])		
Specific weight	[t/m^3]	8.90
Weight	[kg/m]	2.03
Conductor		
Total weight	[kg/m]	3.76
Effective specific weight	[t/m^3]	3.68
Insulation		
Width	[mm]	1.5
Specific weight	[t/m^3]	1.50
Weight	[kg/m]	0.288
Conductor+Insulation		
Total weight	[kg/m]	4.05
Cross section	[mm^2]	1225
Effective specific weight	[t/m^3]	3.31
Current	[kA]	40.25
Current density	[MA/m^2]	32.86

1.2. Superconducting coils

The design principle of the coils is to avoid structural material as much as possible in order to keep the weight of the coils small. The load by mechanical forces must be supported by the intercoil support system. Instead of surrounding the winding pack with a thick steel casing the coil consists of 9 shells, which are welded together thus forming the whole winding pack. The single shell serves as a winding mould for the superconductor. In contrast to a former design [5] the turns are wound in double pancakes consisting of 2x18 turns each (Fig. 6).

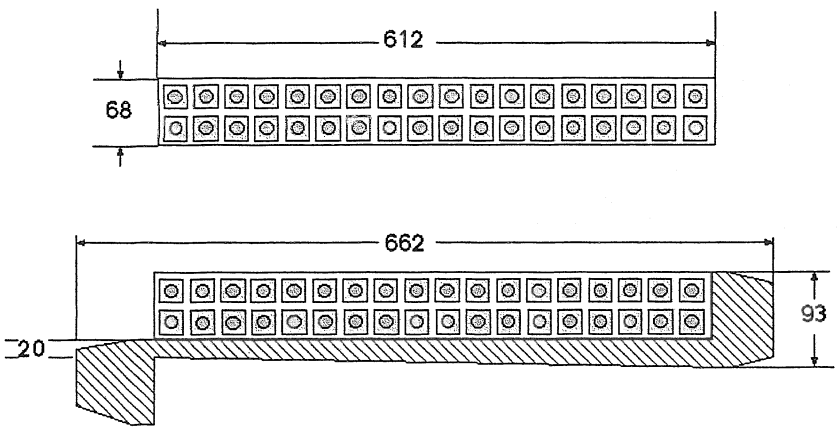

FIG. 6: Double pancake of windings and winding mould.

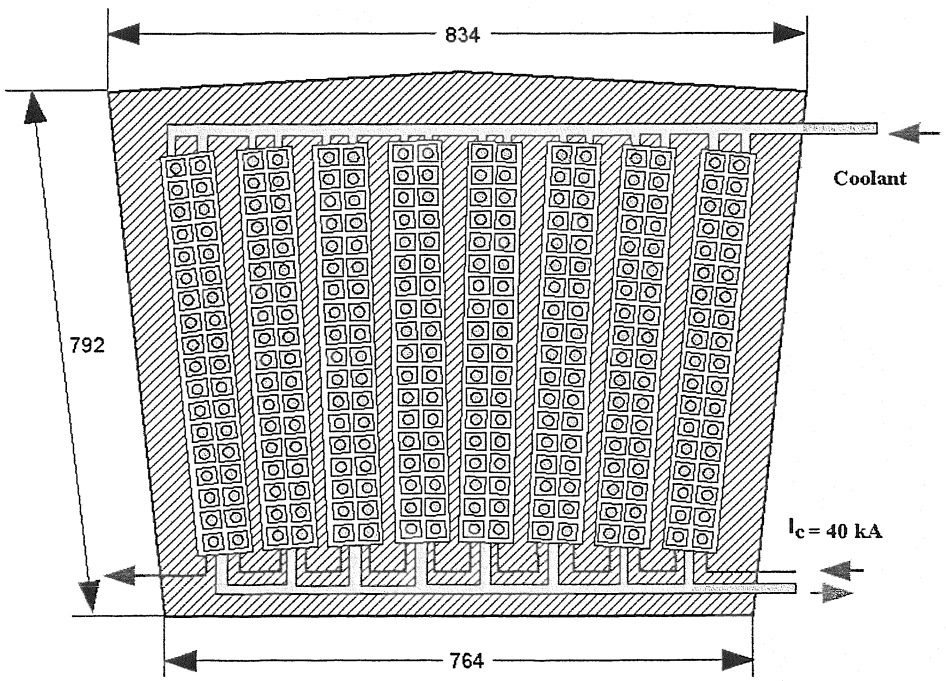

FIG. 7: Cross section of the superconducting coils

The inlet of helium coolant is on the plasma facing side where the deposition by nuclear heat is largest. The cooling length is 612 m. The maximum magnetic field in the coil is 10 T. The weight of the coil is about 108 tonns, details are given in the next table.

Table 2: Main data of superconducting coil

Winding pack		**Casing**	
Av.length of turns [m]	34.50	Width1 [mm]	764
Average radius [m]	5.49	Width2 [mm]	834
Number of turns (18*16)	288	Height [mm]	792
Total length [m]	9936	Total cross section [m^2]	0.6328
Weight [t]	40.30	Cross section of casing	0.24
Width [mm]	560	Volume [m^3]	8.84
Height [mm]	630	Specific weight	7.8
Cross section [m^2]	0.353	Weight of casing [t]	69
Volume of windings [m^3]	12.2	**Coil**	
Imbedding [mm]	10	Total weight [t]	110.8
Cross section [m^2]	0.0238	Weight of SC (NbTi) [t]	20.2
Specific weight	1.8		
Weight [t]	1.478	Total current [MA]	11.6
Total cross section [m^2]	0.38	Av. current density	29.8
Volume of winding pack [m^3]	13.0		
Total weight of winding pack [t]	41.8		

Although the coils differ in shape the data given in Table 2 apply to all coils. The winding length in all coils is nearly the same.

Table 3: Global data of the coil system

Major radius [m]	18	Support structure [t]	4000
Average coil radius [m]	5.49	Gravity support [t]	2000
Number of coils	40	Total weight [t]	10429
Length of conductor [m]	397440	Total current [MA]	463.7
Weight of SC (NbTi) [t]	806.8	Average magnetic field [T]	5.00
Weight of conductor [t]	1316	Magnet. volume [m^3]	10712
Weight of casing [t]	2757	Magnetic energy [GJ]	85
Weight of coils [t]	4429		

The data listed in these tables are consistent with the required magnetic field of 5 T on the axis. Since there is little stray field outside the coil system a simple estimate of the total magnetic energy can be made by taking the volume enclosed by the coils (10700 m^3) and an average magnetic field of 5 T, which yields a magnetic energy of 85 GJ. This number is close to the result of the exact calculation.

The total weight of the coils is 4300 tonns, estimating another 4000 tonns for the intercoil support system and 2000 t for the gravity support of the coils yields a total weight of 10300 tonns. This number is significantly smaller than the weight of the ITER FDR coil system. The amount of NbTi-cable needed in the Helias reactor is 807 tonns, which is roughly the same amount needed for the ITER poloidal field system alone.

1.3. Electromagnetic forces

As a special feature of the modular coils there are strong forces in the lateral direction, which correspond to the overturning forces in a tokamak coil system. These lateral forces can be as large as the radial forces, as can be seen in the next figure.

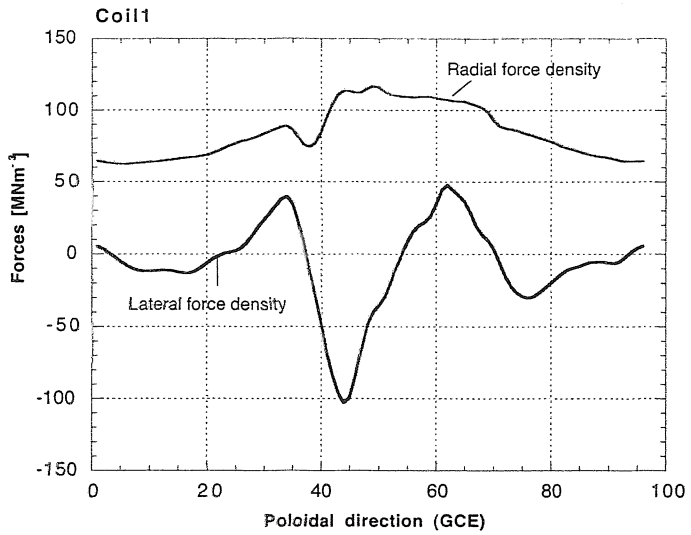

FIG. 8: Radial focres (upper curve) and lateral forces (lower curve) in coil 1 of HSR4/18. The absissa is the number of the finite element along the poloidal direction. The origin is at the outer part of the coil

The largest lateral forces exist in the region where the coils come close together, in particular in the inner toroidal regions these forces are large. The largest lateral force is 100 MNm^{-3}, which corresponds to 63 MNm^{-1}. This force is more than a factor 2 larger than the out-of-plane forces in ITER FDR [6]. The lateral forces in the 5 different coils are shown in the next figure.

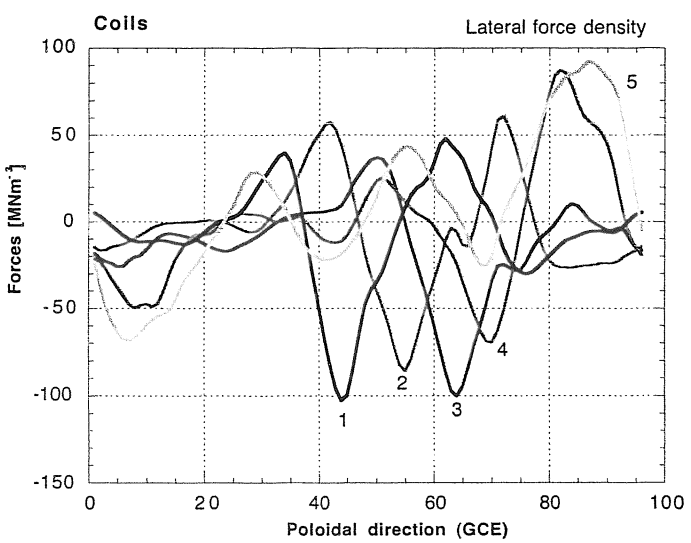

FIG. 9: Lateral forces in 5 modular coils. The number indicates the number of the coils. Coil 1 is the the coil on the left hand side in Fig. 2.

The integrated forces on the coils are not larger than 205 MN, however, the directions of these forces are quite different from coil to coil. Basically the forces are pointing towards the torus center as in a standard solenoid, the integrated force on coil 5, however is rather small and points in the outward direction. The maximum centering force in ITER TF coils is 726 MN, which results from the larger size of the ITER coils and the higher magnetic field. The following table lists the integrated force on the coils in HSR4/18.

Table 4: Total forces on the coils in one period. The numbering of the coils is described in Fig. 2.

Coil	Fx [MN]	Fy [MN]	|FR| [MN]	Fz [MN]
1	-181.5	-95.8	205.2	-44
2	-130	-87.4	157.3	-61.7
3	-78.2	-142.9	162.9	-129.9
4	-77.9	-65.4	65.9	-107.8
5	14.6	18.6	23.6	-43.9
6	14.6	-18.6	23.6	43.9
7	-77.9	65.4	65.9	107.8
8	-78.2	142.9	162.9	129.9
9	-130	87.4	157.3	61.7
10	-181.5	95.8	205.2	44

The maximum centering force is |FR|=205 MN, this maximum occurs on coil 1, the centering force on the other coils is smaller. The vertical component of the force vector can reach 50% of the maximum centering force; the maximum is reached on coils 3 and 8, which are shifted in opposite directions. This gives rise to tilting forces on the total coil system, which must be compensated by an appropriate support system.

3. Magnetic field of the Helias reactor

Magnetic surfaces of the vacuum field in HSR4/18 are shown in Figs. 10 and 11. The rotational transform ranges from 0.83 in the center to 0.96 at the boundary. There is a shallow vacuum magnetic well of roughly 1%, which deepens with rising plasma pressure to 7.5% at $\langle\beta\rangle$ = 4.3%. Outside the last magnetic surface, which has an average radius of 2m, the magnetic field is stochastic. This stochastic region is the remnant of the 4 islands at $\iota = 1.0$, however the basic structure of the 4/4-islands is still present and the plasma flow in this region will follow well defined channels towards the divertor target plates. In the bulk plasma there are no significant magnetic islands, except for $\iota = 8/9$, where 9 small islands exist.

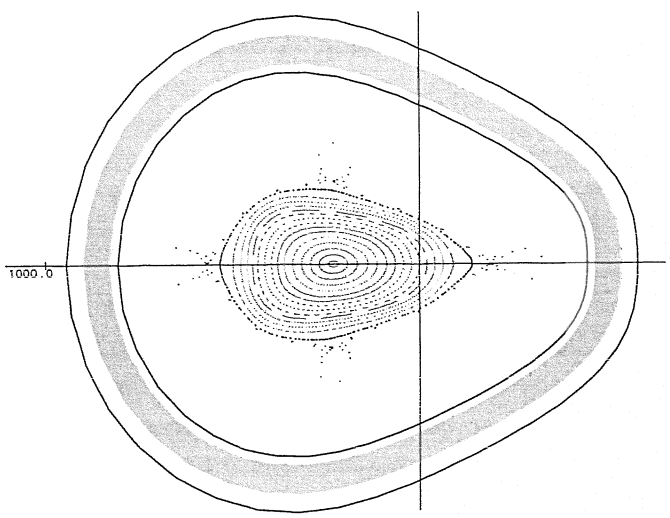

FIG. 10: Poincaré plot of magnetic surface in the plane φ=45°. Vacuum field

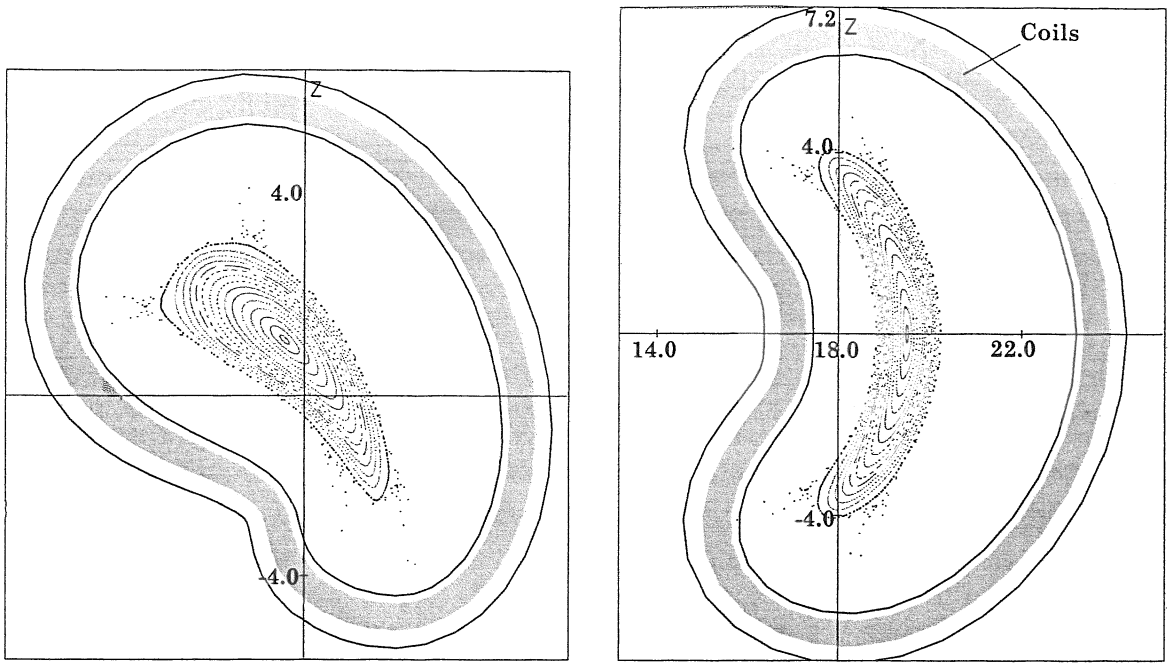

FIG. 11 Poincaré plot of HSR18, vacuum field. Left: symmetry plane φ=22.5°, right: symmetry plane φ=0°. Units in m. The region between plasma and coils is available for blanket, shield and first wall.

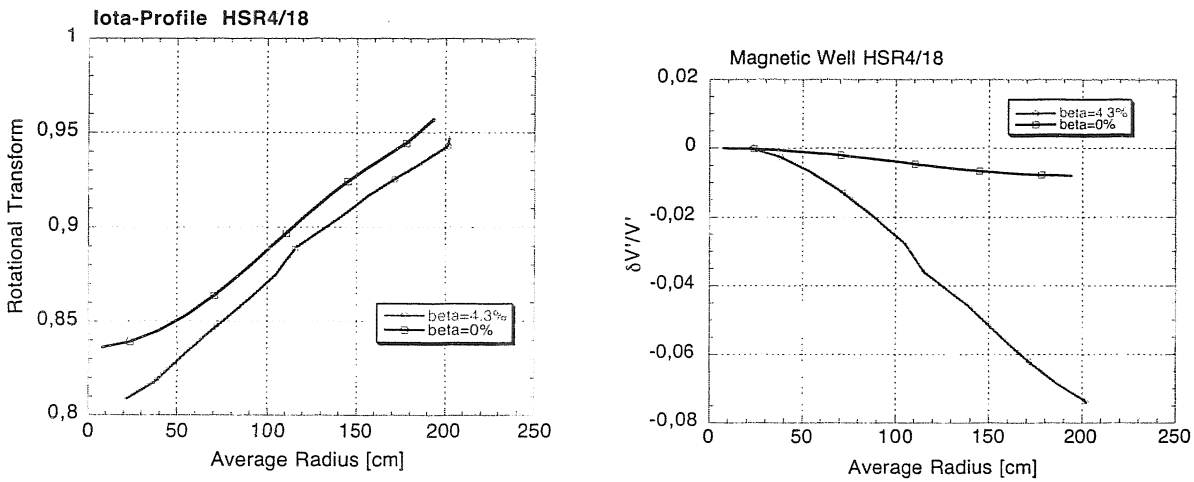

FIG. 12: Left: Rotational transform vs average radius, upper curve: vacuum field, lower curve beta = 4.3%. Right: Magnetic well in vacuum case (upper curve) and finite beta (beta = 4.3%, lower curve).

4. Plasma Equilibrium

The MHD-equilibrium has been computed using the NEMEC code and the MFBE-code [7]. A basic feature of the Helias configuration is the reduction of the parallel plasma currents – the Pfirsch-Schlueter currents - to a small level. As a result of this optimisation the Shafranov shift in the finite beta equilibrium is very small. This effect could be verified in HSR4/18 to a large extent. Current lines on a magnetic surface are shown in the following figure (Fig.13). In some regions the current flows nearly perpendicular to the field lines indicating small

parallel current density in this place. The maximum ratio between parallel current density and diamagnetic current density is 1.6, on average the ratio is 0.7.

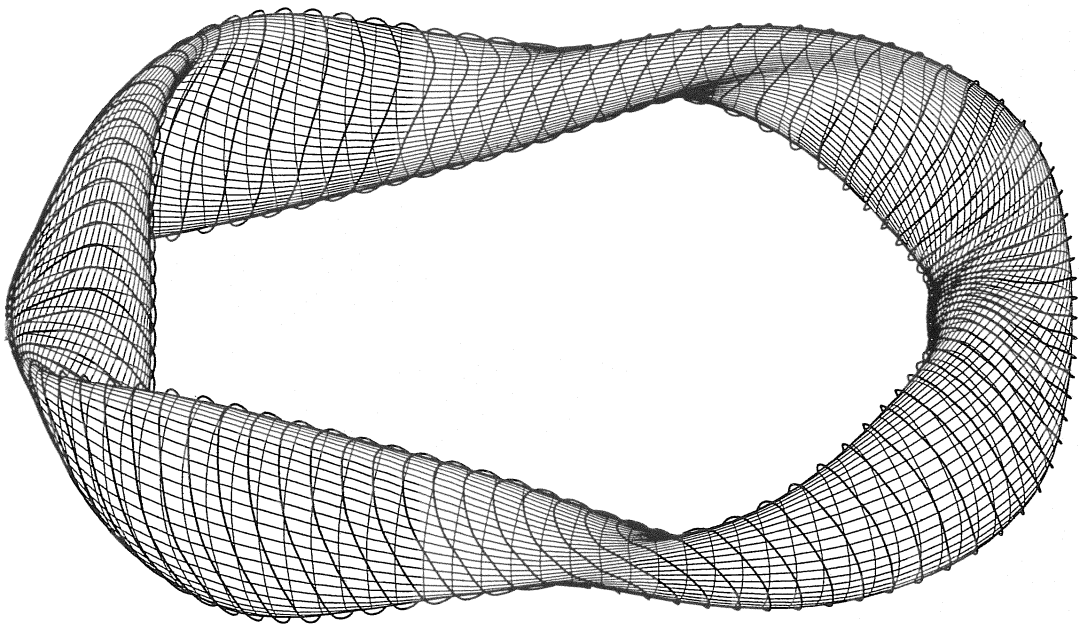

FIG. 13 :Magnetic surface of HSR4/18. The thick solid lines are the plasma current lines.

The results shown in the next figures verify the small Shafranov shift at $<\beta> = 4.3\%$.

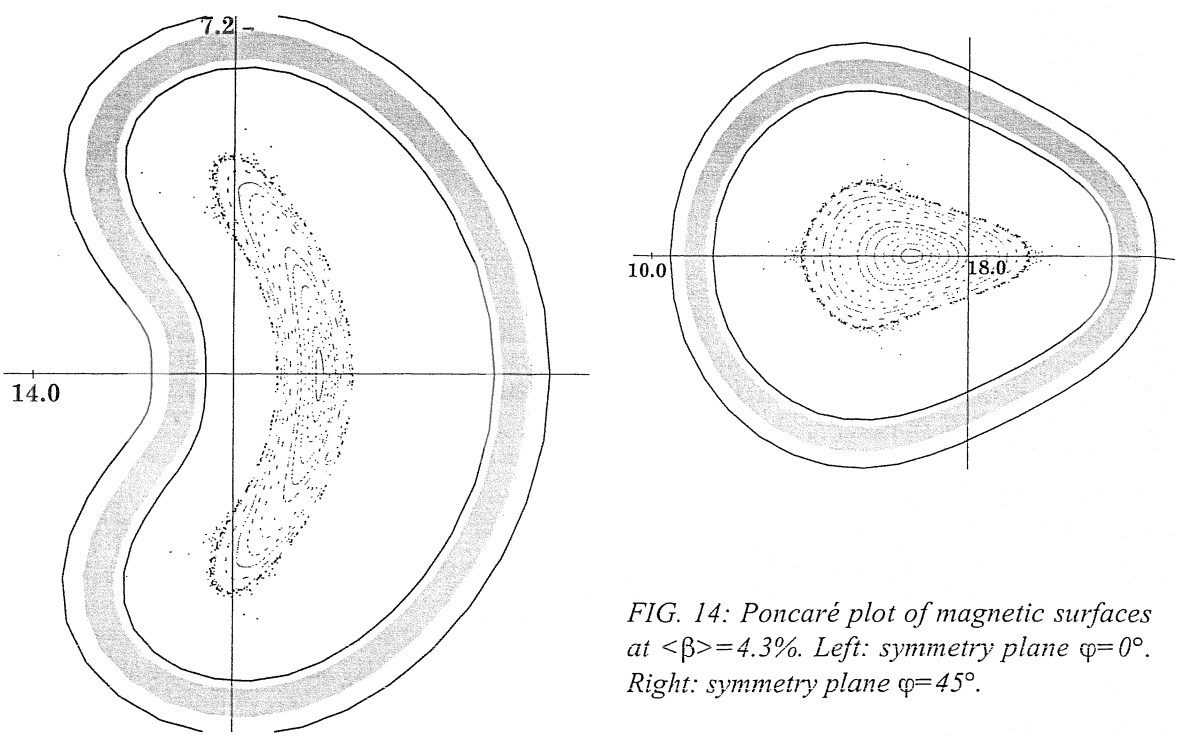

FIG. 14: Poncaré plot of magnetic surfaces at $<\beta>=4.3\%$. Left: symmetry plane $\varphi=0°$. Right: symmetry plane $\varphi=45°$.

The rotational transform in the finite beta case is slightly reduced compared with the vacuum case (see Fig. 12). This implies that the position of the islands at the plasma boundary also varies with increasing beta, which must be taken into account in designing the divertor geometry.

5. Plasma stability

Numerical investigations of the MHD-stability in HSR5/22 have shown stability up to an averaged beta of 4% [8]. This result was found by local ballooning mode analysis using the JMC-code and by global mode analysis with the CAS3D code [9]. Both methods yield instability at $<\beta>=5\%$. Interpolating the results of CAS3D results in a stability limit of 4.2% [10].Low-order rational magnetic surfaces, which do not exist in the vacuum field, can exist in the finite beta plasma. This concerns the 5/6 resonance, which appears for $<\beta> \geq 4.2\%$. In order to prove MHD-stability at the design point of $<\beta> = 4.2\%$, detailed computations of the equilibrium and careful optimisation of the pressure profile are necessary.

Stability analysis using CAS3D has shown that the equilibrium of HSR4/18 depicted in Fig. 14 is unstable against global modes in the boundary regions, while at $<\beta> = 3.5\%$ these modes are stable. There is a chance that by tailoring the pressure profile global modes can also be stable at $<\beta> = 4.3\%$. As shown in Fig. 12 the rotational transform in HSR4/18 decreases slightly in the finite β–case. Above $<\beta> = 4.3\%$ it is expected that the resonant surface at $\iota=4/5$ exists in the plasma center. Since the global modes found in HSR4/18 occur in the boundary region this may be of no relevance in the context of stability.

Stellarator experiments show that even below the MHD-stability limit the plasma is unstable and this instability leads to anomalous transport of particles and energy. Resistive drift- and resistive ballooning modes are candidates for this effect. Drift waves in the linear and non-linear approximations have also been studied numerically taking into account the specific geometry of the Helias configuration. In particular, attention has been focussed on the effect of field line curvature and local shear on the linear growth rate of the dissipative drift waves. The larger local shear in Helias configurations, which is a by-product of the optimisation process, has a stabilising effect on the drift waves [11].

6. Neoclassical Transport

The Helias reactor is expected to operate at high density (central electron density of $3\text{x}10^{20}$ m^{-3}) and moderate temperature (central temperatures of 15 keV). Under these conditions, neoclassical theory predicts that only the so-called 'ion-root' solution for the radial electric field exists, thus demanding strong optimisation of the magnetic field spectrum to minimize losses in the stellarator-specific $1/\nu$-regime. HSR4/18 is excellent in this regard, having an effective helical ripple considerably less than one per cent over the entire plasma cross section (see Figure 15). At this level, $1/\nu$-losses pose no threat to ignition.

The design philosophy of the Helias concept is to minimize the bootstrap current so as to avoid the possibility of low-order rational values of rotational transform within the confinement volume and to maintain a fixed edge topology of the magnetic field structure to insure the proper functioning of the divertor. Initial calculations indicate that HSR4/18 would have a bootstrap current significantly less than that of the equivalent axisymmetric device but further investigations are required to ascertain whether this reduction is sufficient.

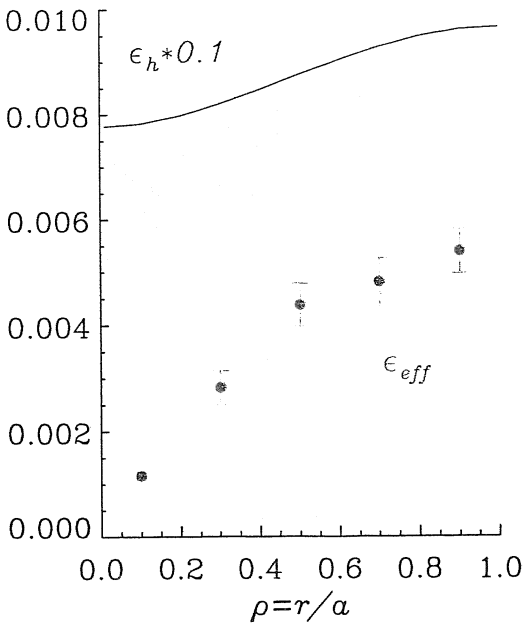

FIG. 15: Numerical results for the effective helical ripple for 1/ν-transport, ε_{eff}, are shown as a function of normalized minor radius. For comparison, the geometric value of the helical ripple, ε_h, is also shown (reduced by a factor of 10). For a classical stellarator, ε_{eff} and ε_h are equal.

7. Alpha-Particle Confinement

The magnetic field spectrum of the Helias reactor is chosen so that the device becomes a true minimum-B configuration at operational values of plasma pressure, thereby providing good confinement of fast α-particles [12]. This effect has been verified in HSR4/18 by following the guiding center orbits of 1000 α-particles, launched according to the expected density and temperature profiles, for approximately one slowing-down time (0.13 seconds for the chosen parameters). The α-particles start with an inital energy of 3.52 MeV but then experience pitch-angle and energy scattering during the simulation. The results confirmed that no direct losses are present (the earliest losses occurring after roughly 10^{-2} seconds) but that stochastic diffusion due to particles trapping/detrapping in local ripple wells leads to a lost-energy fraction of ≈2.5% in HSR4/18. This is considered tolerable with respect to the energy balance of the reactor, however, the impact of the highly energetic α-particles on the first wall could be a matter of concern.

Energetic α-particles can excite Alfvén instabilities, which may cause enhanced losses of these particles and, thus, reduce the heating efficiency. Therefore, the structure of the Alfvén continuum in HSR4/18 was studied, Alfvén eigenmodes residing in the continuum gaps were investigated, and possible energy losses associated with the escaping of circulating and transitioning α-particles were evaluated. It was found that the largest losses can result from destabilization of Mirror-induced Alfvén eigenmodes (MAE) and helicity-induced Alfvén eigenmodes with the poloidal and toroidal mode coupling $\Delta\mu=\Delta\nu=1$ (HAE_11). It was shown that the destabilization of certain Alfvén eigenmodes affects transport of the partly slowed down alphas, thus promoting the removal of the helium ash from the reactor. Computations of single particle orbits under effect of Alfvén waves have confirmed this effect [13].

8. Divertor Concept

Although the structure of the magnetic field outside the last closed surface is stochastic there exists a separatrix region of the 4/4–islands, where a strong radial transport of the outflowing plasma arises. The structure of this inhomogeneity has been investigated by Monte-Carlo technique following particles along field lines subject to pitch angle scattering. Anomalous transport and radial spreading of the scrape-off layer is simulated by a collision frequency leading to an effective diffusion coefficient of D=1 m^2/s. This technique allows one to optimise the shape and the position of the target plates.

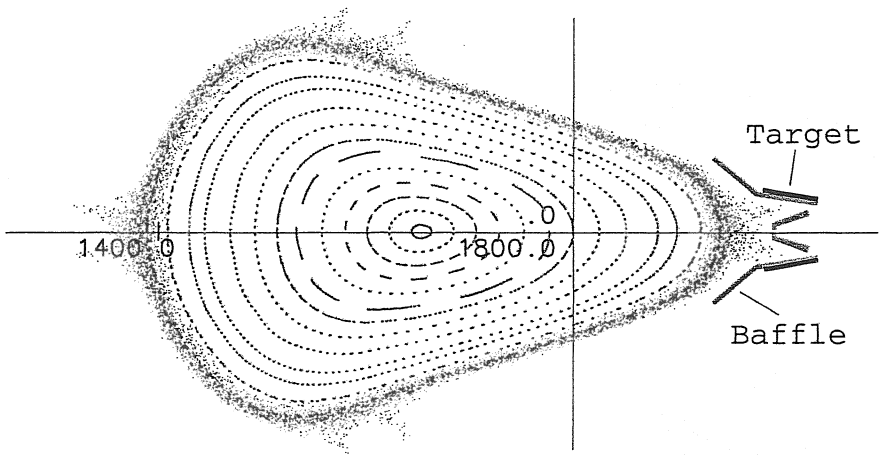

FIG. 16: Poincaré plot of magnetic surfaces and scrape-off layer in the symmetry plane φ=45°. The stochastic region is created by intersection points of diffusing particles.

As Fig. 16 shows, radial diffusion is strong in some specific regions, which quite naturally are selected for positioning target plates. The purpose of the baffle plates is to confine the recyling neutrals. Toroidally the target and baffle plates extend until the next symmetry plane as shown in Fig. 17.

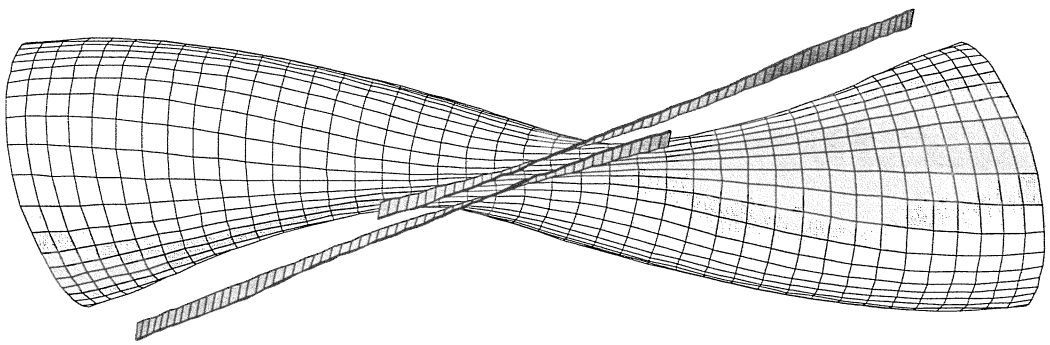

FIG. 17: HSR4/18. One period of a magnetic surface and divertor target plates seen from outside. Baffle plates are not shown.

Heat load on the target plates is a critical issue; preliminary computations indicate a thermal load of more than 10 MW/m^2. This figure is too large as a steady state load and therefore methods have to be explored, how a detached plasma and a radiative boundary layer can be realized, which allows one to reduce the thermal load onto the target plates to approximately to 5 MW/m^2. This is a common issue for tokamaks and stellarators.

9. The Helias Reactor as a Power Plant

First steps are being made to develop an integrated concept of the stellarator power plant including the buildings and the thermal conversion cycle. The coil system is enclosed in a cryostat of roughly 16 x 16 m^2 cross section (see Fig. 18). The volume of the cryostat in HSR4/18 is 21500 m^3. This volume is smaller than the volume of the ITER cryostat.

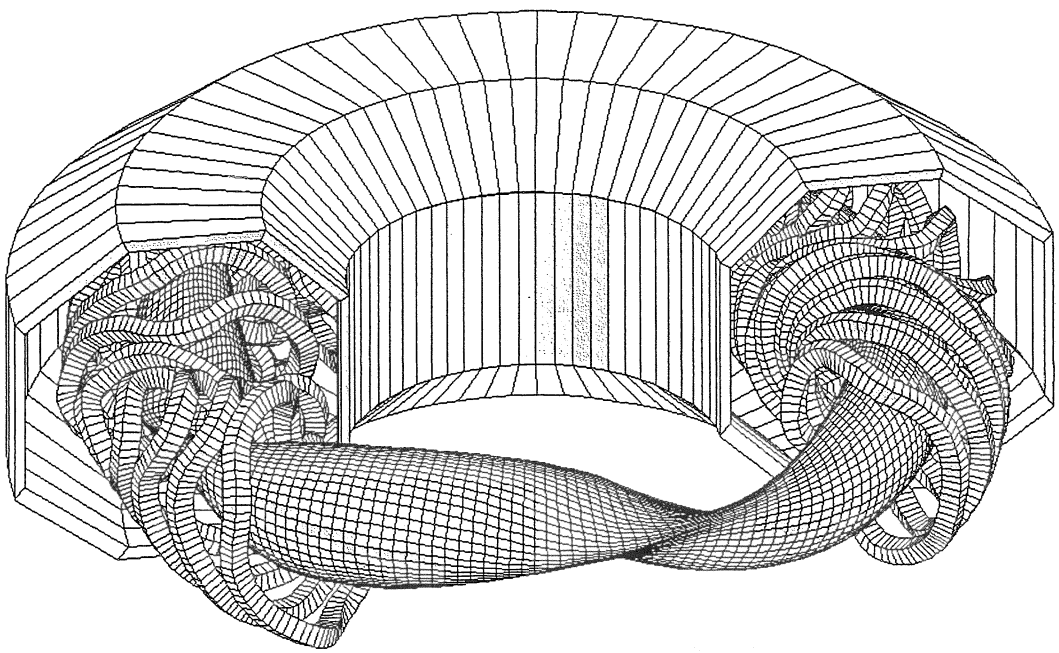

FIG. 18: Plasma, coils and cryostat of HSR4/18. The inner diameter of the cryostat is 20 m.

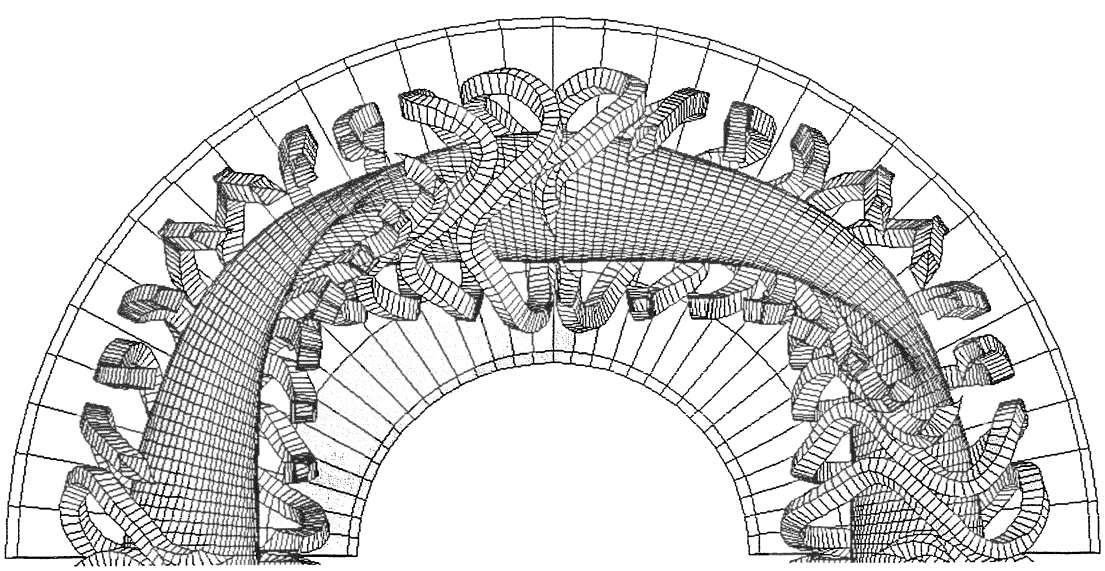

FIG. 19: Cut-away of the cryostat with coils and plasma. The diamater of the inner bore is 20 m, the outer radius of the cryostat is 26 m.

Enclosed in the cryostat is the coil system and its support system. Furthermore it contains the vacuum vessel, the blanket and the plasma facing components. The inner bore of the cryostat is 20 m. This space may be utilised for the power supply of the coils and the feeders of the helium cooling. Furthermore there is space available for ECR-heating from the high field side. The estimated amount of ECR-heating power is 100 MW, which can be fed into the plasma through 10 wave guides, which enter the inner bore from below and launch the ECR-power from the high field side into the plasma. This plasma heating is needed only in the start-up phase, while in the steady state burn phase the external heating is switched off and the port holes for heating are closed. On the outside of the cryostat the heat exchanger and the pellet injector are located. The Fig. 19 shows a cut-away of the cryostat depicting the coils and the plasma column.

Due to the large average major radius of 18 m the wrong impression may be made, that stellarator reactors must be large in all directions and thus require higher capital investments than in a tokamak reactor. To illustrate the relation to a tokamak of reactor size the next figure shows ITER FDR and HRS4/18 on the same scale.

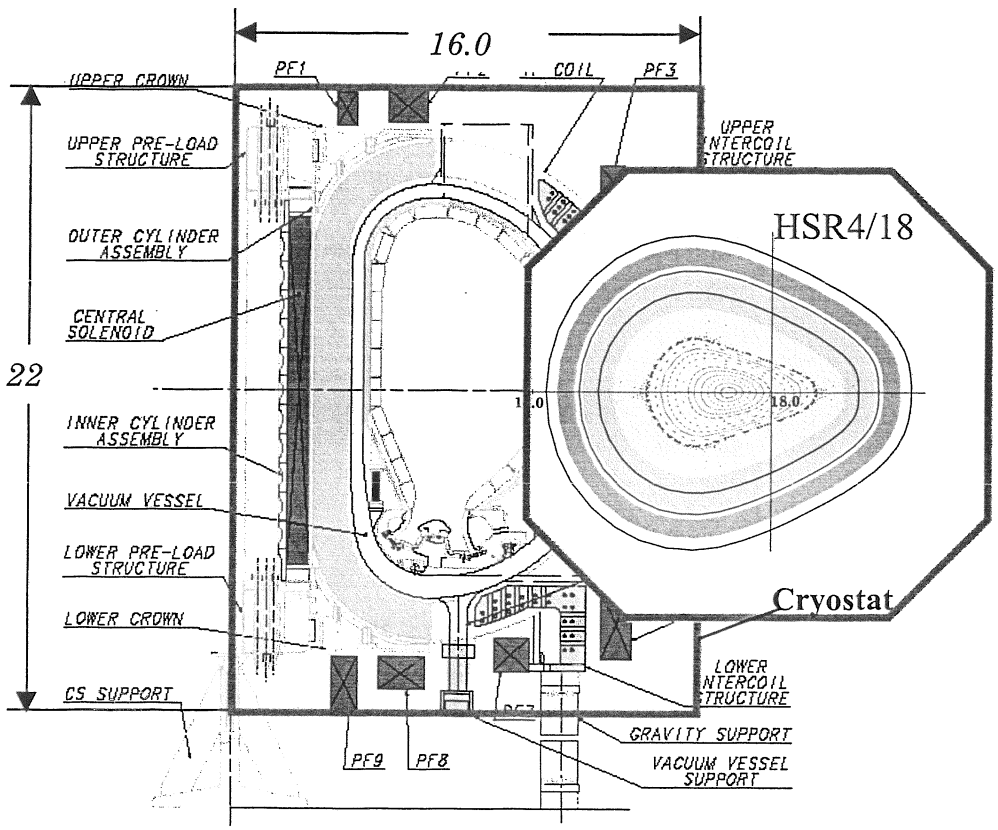

FIG. 20: HSR4/18 and ITER FDR.. The volume of the cryostat in HSR4/18 is smaller than in ITER

1.4. Maintenance

In contrast to earlier concepts of maintenance and repair, in which a whole period of the coil system is horizontally withdrawn [14], it is proposed to replace blanket segments through portholes between the coils. In every period there are 8 big portholes available, 4 on the top

and 4 at the bottom of the period. Typical dimensions of the portholes are 2x6 m^2. The following figure shows the arrangement of the portholes.

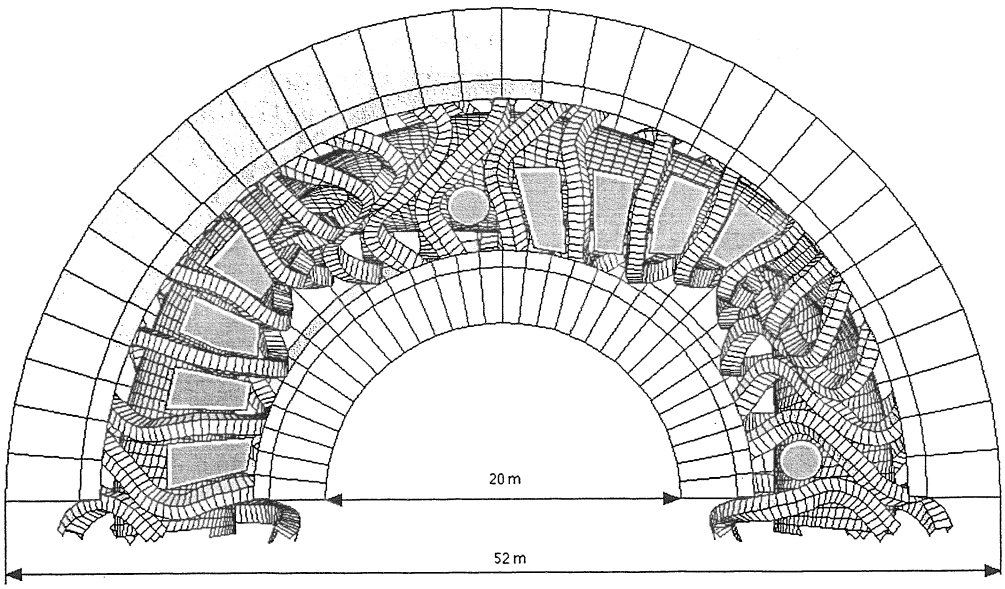

FIG. 21: View from the top onto half of HSR4/18 showing the portholes for maintenance.

Further access is possible through horizontal portholes, which are as large as the vertical ones.

1.5. Blanket

The blanket options envisaged in the Helias reactor are:

Helium-cooled solid breeder blanket (HCPB)
Water-cooled Li-Pb blanket (WCLL)

Two major differences between a tokamak reactor and a Helias reactor are decisive with respect to blanket design and performance. These are the three-dimensional shape of the blanket and the larger area of the first wall. In the present concept of HSR5/22 this area is 2600 m^2, which leads to an averaged neutron wall loading of less than 1 MW/m^2 (neutron power 2400 MW). The peak wall loading is 1.7 MW/m^2. As the result the lifetime of first wall and structural components is larger than in a compact tokamak reactor. Compared with the DEMO tokamak reactor, where a lifetime of 2.3 years [15] (70 dpa in the structural material) is envisaged, the lifetime of blanket elements can reach 4.6 years. Since in recent studies a limit of 140 dpa is considered realistic [16], the lifetime of components in the Helias reactor may reach 9 years. In HSR4/18 the area of the first wall is 2500 m^2, which results in a slightly higher average neutron wall load than in HSR5/22.

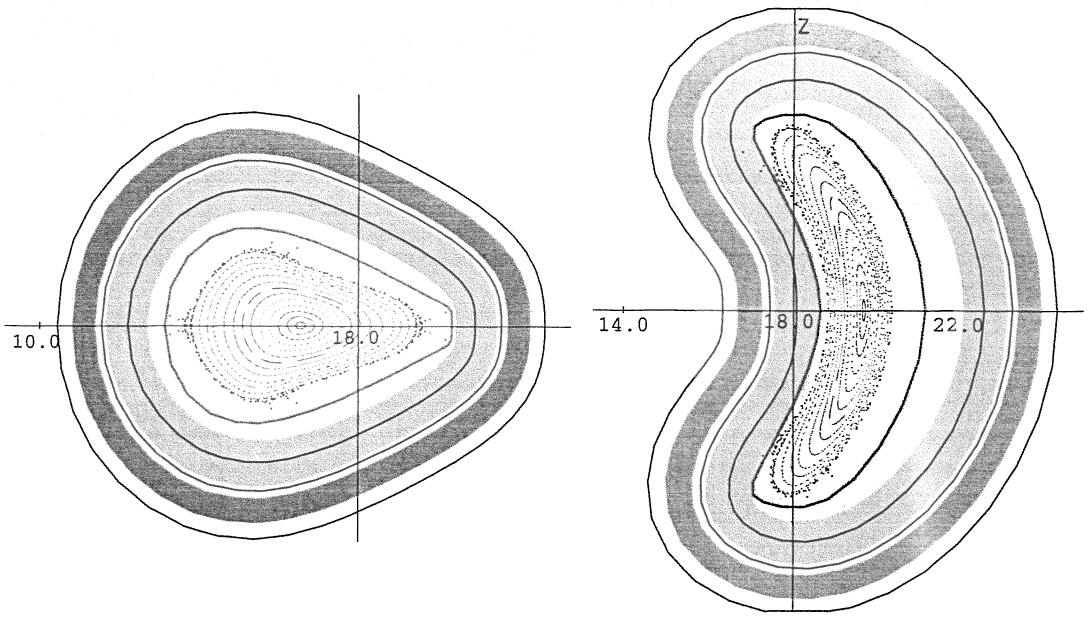

FIG. 22: Cross section of coils, blanket, first wall and magnetic surfaces. The area of the first wall is 2500 m^2.

The distribution of highly energetic neutrons on the first wall is very inhomogeneous; there exists not only a poloidal inhomogeneity but also a toroidal variation of the neutron flux. In the triangular plane ($\varphi = 45°$) it is rather homogeneous, however, in the plane with a bean-shaped plasma cross section the horizontal regions are heavily loaded while in the vertical direction the neutron power load is very small. The distribution is shown in the following figure.

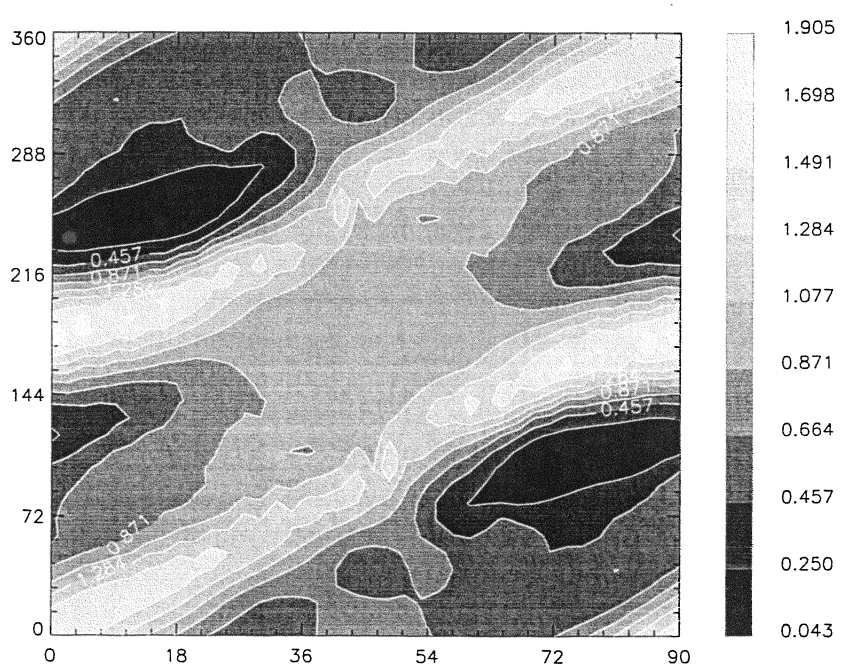

FIG. 23: Map of the nuetron power load on the first wall of the Helias reactor HSR4/18. The abcissa is the toroidal angle and the vertical axis denotes the poloidal angle. The origin is located at $\varphi=0°$ and in the plane $z=0$.

The maximum of the neutron power is 1.9 MWm^{-2} and this peak occurs on the inboard side of the first wall. As in the Helias reactor HSR5/22 the assumed total fusion power is 3000 MW.

The following table summarizes the data of neutron wall loading in HSR5/22 and HSR4/18.

Table 5: Power flow onto first wall

		HSR4/18	HSR5/22
Neutron power	[MW]	2400	2400
Area of first wall	[m^2]	2500	2600
Average neutron power load	[MW/m^2]	0.96	0.92
Peaking factor		1.98	1.7
Peak power loading	[MW/m^2]	1.9	1.56
α-Particle heating power	[MW]	600	600
Radiation (50% of P_{alpha})	[MW]	300	300
Radiative wall loading (av.)	[MW/m^2]	0.12	0.12
Power to target plates	[MW]	300	300

As in any toroidal fusion device the purpose of the blanket is to provide sufficient breeding of tritium and to shield the superconducting coils against neutrons. Since atomic processes determine the size of the blanket, its radial width is an absolute figure and any fusion device has to provide enough space to accomodate a blanket with about 1.3 m radial build. In contrast to tokamaks the stellarator, however, requires a 3-dimensional design of the blanket, which must conform to the 3-dimensional shape of the plasma. Blanket segments must be small enough to be replacable through portholes, therefore a stellarator needs a large variety of different modules, which in the case of the Helias reactor HSR4/18 is 200 (50 segments in every period) comprising 25 different shapes. The various blanket concepts, which have been studied for tokamak reactors [17], are also suited in stellarators. Either a solid breeder blanket (HCPB [18]) or a liquid LiPb blanket with additional cooling [19] are the options in the Helias reactor HSR5/22 [20].The most attractive option for HSR5/22 is the self-cooled LiPb blanket with additional helium cooling. This concept provides high efficiency of the thermal cycle and avoids the hazards associated with water-cooling or the use of large amounts of beryllium. The large weight of the LiPb is a drawback, however the liquid breeder material is reusable and hence not considered as nuclear waste. This also holds for beryllium, which must be reprocessed and separated from the tritium.

The weight of the blanket and shield depends on the specific concept, first estimates for HSR5/22 [21] resulted in an overall weight of 7080 t for a HCPB-blanket and 14450 t in case of a water-cooled Li-Pb- blanket. In this case the breeder material alone weighs 12500 t.

The lifetime of first wall and blanket depends on the neutron fluence and the limits of the structural material. The MHH-study [24] assumed a limit of 200 dpa of the vanadium alloys corresponding to a lifetime of the blanket of 11 years. The end-of-life fluence is 16.4 MWy/m^2 (peak) and an average fluence of about 9.1 MWy/m^2. Given these optimistic assumptions the lifetime of the blanket in HSR4/18 (also equipped with V-alloys) would be 13.5 years. Here it is assumed that the availability of the reactor is 76%. More conservative studies of blanket performance [ref 16] assume a maximum average fluence of 6 MWy/m^2, which would lead to a lifetime of 9 years in the Helias reactor.

10. Power balance

Power balance in the Helias reactor HSR5/22 has been studied by various methods: local transport calculations using the ASTRA-code and the TOTAL_P-code, and extrapolation of empirical scaling laws of stellarator confinement to reactor conditions [22]. Although

HSR4/18 differs from HSR5/22 in the magnetic field geometry, magnetic field strength and plasma volume are nearly the same. Therefore empirical scaling laws predict nearly the same confinement times for both reactor concepts. In modeling a fusion plasma in stellarators the radiative density limit [23] must be taken into account. Extrapolating experimental results from Wendelstein 7-AS allows one to model a fusion plasma with peak density of $3*10^{20}$ m^{-3} and a temperature of 15 keV. A self-consistent set of parameters is listed in the following table.

TABLE II: Plasma parameters in HSR4/18

	HSR4/18(1)	HSR4/18(2)	
Magnetic Field	5.0	5.0	[T]
Line Average Density	$2.42\ 10^{20}$	$2.6\ 10^{20}$	[m^{-3}]
Electron Density n(0)	$2.64\ 10^{20}$	$2.84\ 10^{20}$	[m^{-3}]
Electron Temperature T(0)	12	15	[keV]
Av. Electron Temperature	3.97	4.96	[keV]
Plasma energy	744	981	[MJ]
Beta(0)	10.0	13.2	[%]
Average Beta	3.18	4.2	[%]
Energy Conf. Time (required)	3.2	2.3	[s]
Energy Conf.Time (LGS)	3.26	2.35	[s]
Energy Conf.Time (W7)	4.23	3.14	[s]
Energy Conf.Time (ISS95)	2.07	1.5	[s]
Bremsstrahlung	100	144	[MW]
Fusion Power	$1.75\ 10^{3}$	$3.0\ 10^{3}$	[MW]

In the second column this table shows the design point at a fusion power of 3000 MW. The beta value of 4.2% is at the limit of MHD-stability as outlined above. Ignition, however, is possible at lower values of beta, in HSR4/18 ignition occurs at $<\beta> = 3.2\%$. As shown in Table II, the empirical scaling time (LGS = Lackner-Gottardi scaling) meets the required confinement time, while the ISS-scaling predicts a confinement time, which is too low.

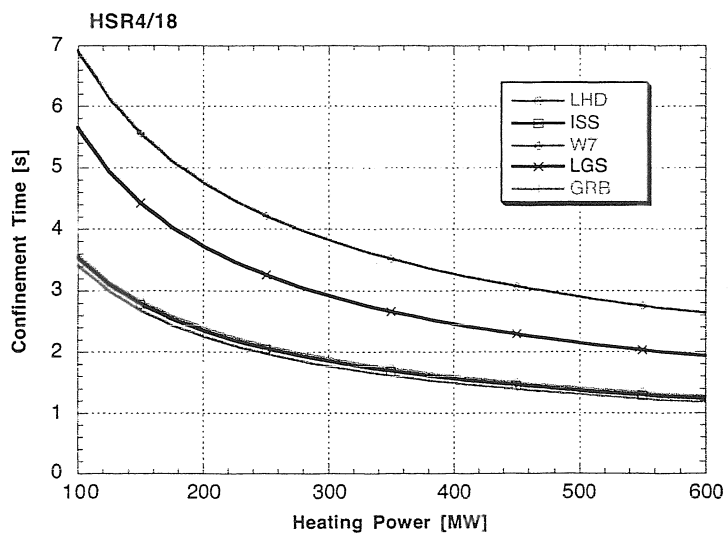

FIG. 24: Empirical energy confinement times vs internal heating power in HSR4/18. ISS= International stellarator scaling, LHD=LHD-scaling, GRB=Gyro Bohm scaling

Figure 24 shows the confinement times predicted by various scaling laws as function of the heating power. The confinement time W7 is a best fit to the data of Wendelstein 7-AS. Extrapolating this scaling towards the Helias reactor yields confinement times, which are appreciably larger than the reqired ones (upper curve in Fig. 24). The heating power is the alpha-particle heating power reduced by the radiation power, the external heating power is zero. The confinement time, which is needed for self-sustained burn is 2.3 s. This time is defined as the ratio between plasma energy (981 MJ) and the net heating power (431 MW). The ignition margin is the ratio between the confinement time from scaling laws and the required confinement time. Self-sustained burn is possible if this ratio is larger than unity.

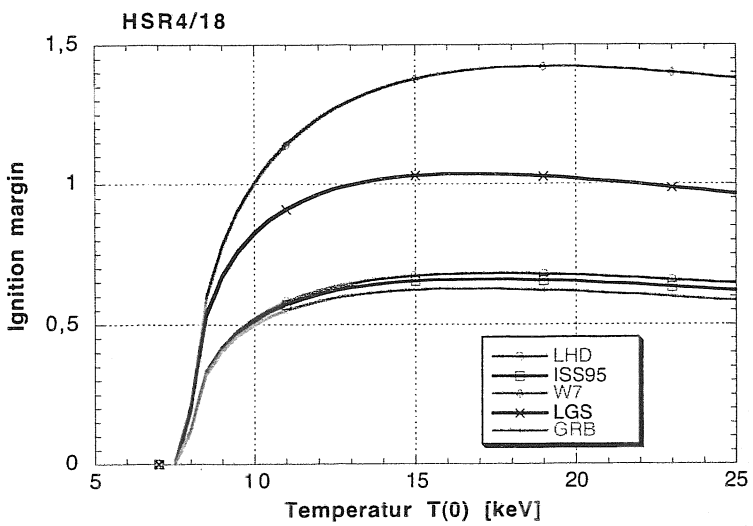

FIG. 25 Ignition margin vs peak temperature in HSR4/18

To compute this ignition margin the plasma profiles have been kept fixed. Below T(0) = 10 keV the discharge cannot be sustained by internal heating alone, however at T(0) = 13 keV the ignition margin according to the LG-scaling law is above unity and external heating is no longer needed. If the confinement would follow the W7-scaling this point will be reached at 10 keV. At T(0) = 13 keV the average plasma beta is 3.2 %, which is below the MHD-stability limit. The fusion power output under these conditions is 1.75 GW.

These estimates show that the requirement of an economic fusion power output of 3000 MW is compatible with the envisaged physics properties of the Helias reactor HSR4/18. If the confinement times in HSR4/18 follows the LG-scaling or the W7-scaling no enhancement factor is needed.

11.The thermal cycle

Most of the thermal power is carried by neutrons to the blanket (P_N = 2400 MW) and after having passed the heat exchange system the thermal power is converted to electricity P_E (efficiency η_c). In the blanket nuclear processes enhance the thermal power described by a blanket multiplication factor η_B, which is between 1.2 –1.4 depending on the blanket design. The α-heating power (P_α = 600 MW) finally ends on the divertor target plates by charged particles and on the first wall in the form of bremsstrahlung or – if a detached plasma can be maintained – as impurity radiation. The power onto the first wall is recovered in the cooling circuit and added to the blanket power. Let η_w be the fraction of α-power dumped on the first wall and 1 - η_w the fraction to the divertor, then the total thermal power is

$$P_{th} = \eta_B P_N + \eta_w P_\alpha + \eta_D(1-\eta_w)P_\alpha \qquad \text{Eq. 1}$$

η_D is the efficiency of the divertor cooling. To improve the overall efficiency of the power plant the cooling power of the divertor plates must be included in the total thermal power. To avoid two separate cooling circuits the blanket and the divertor use the same inlet temperatures.

As in tokamak reactors the stellarator reactor needs a certain fraction of recyling power to feed all consumers of electricity in the power plant. The main part goes into the cooling system of the coils and into the pumps of the blanket cooling system. This power is dumped to the environment as low-grade heat, however the power to the cooling pumps can be recovered with a certain efficieny and reused in the primary coolant loop. Recirculating power, which is used in vaccum pumps, tritium recovery system, pellet injection system, control systems etc. is certainy not recoverable and will be dumped as thermal waste. A simplified power flow diagram of the stellarator reactor is shown in the next figure

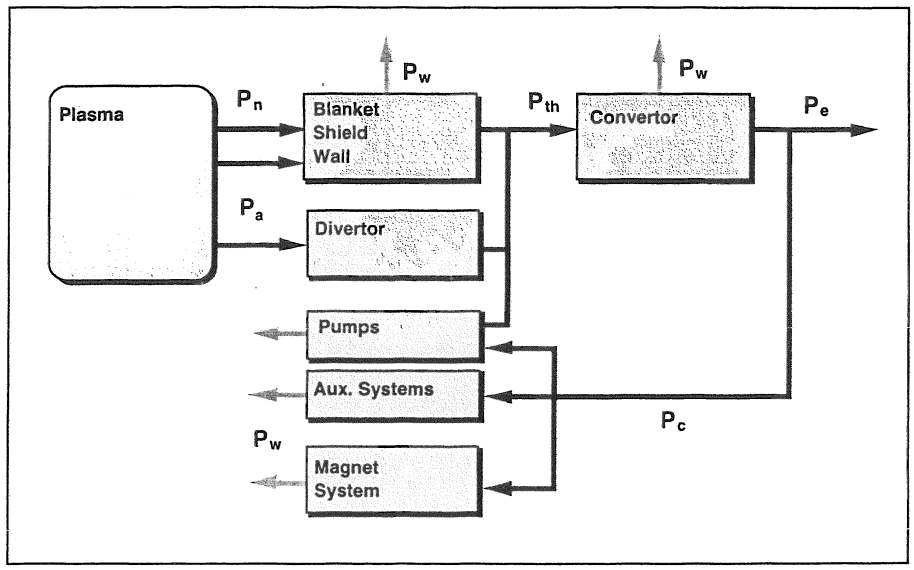

FIG. 26: Power flow diagram in a stellarator reactor

Electricity output depends crucially on the thermal conversion efficiency of the convertor and on the outlet temperature of the cooling system. The MHH power plant study (SPPS [24]) assumes an outlet temperature of 610 °C, which allows a conversion efficiency of 46%. This efficieny can be reached with the advanced Rankine cycle as proposed in the ARIES tokamak reactor studies [25]. The allowable temperature of the structural material sets a limit to the temperature in the thermal cycle. The choice in the SPPS study is vanadium alloy (V5Cr5Ti) where the limits are 650-750°C.

The thermal power balance and the efficiency of plant depend strongly on the choice of the breeder and the structural material. A helium-cooled liquid lead blanket was proposed in the ASRA-6C study [26] leading to an overalll efficiency of 42.7 %. To achieve a sufficient breeding ratio a large amount of beryllium had to be added in the blanket, which is a disadvantage from the point of view of safety. With respect to blanket, structural material and cooling cycle there is no difference between the modular ASRA-6C stellarator and a modern Helias stellarator. Blanket options, which have been designed for tokamak reactors, can also be used is stellarators; however, the three-dimensional shape the plasma requires also a three-

dimensional shape of the blanket. Lowest efficiency is achieved with a water-cooled LiPb-blanket. The following table lists the data of a Helias reactor for various blanket concepts.

Table 6: Power flow in a Helias reactor

Fusion power	[MW]	3000
α-power	[MW]	600
Neutron power	[MW]	2400
Self-cooled LiPb-blanket		
Multiplication factor		1.3
Thermal power	[MW]	3720
Conversion efficiency		0.46
Gross electric power	[MW]	1711
Recycling power	[MW]	95
Net electric power	[MW]	1625
Thermal waste	[MW]	2008
Water-cooled LiPb-blanket		
Multiplication factor		1.2
Thermal power	[MW]	3480
Conversion efficiency	[MW]	0.35
Gross electric power	[MW]	1218
Recycling power	[MW]	95
Net electric power	[MW]	1123
Thermal waste	[MW]	2262

12.Safety issues of the stellarator reactor

Many results of the SEAFP-study by J. Raeder et al.[27] can be extrapolated to a stellarator reactor since the total number of neutrons produced per second, which is 10^{21} n/s in a 3000 MW reactor, is a function of the envisaged fusion power alone. This implies that the integrated effects of the neutrons in the structure and thus the amount of nuclear waste and the the associated issues are the same in both reactor types. On the other hand, stellarator and tokamak reactors differ in size, coil system and size of the blanket, which has some consequences for the safety issues. Tritium inventory and possible mobilisation of tritium by accidents is a main issue in any fusion reactor.

According to the principle of defence in depth the first step is to avoid possible sources of failure and hazards. In a stellarator the magnetic energy stored in the coil system and the energy in the plasma are rather small compared with tokamak power plants. In the Helias reactor HSR44/18 the overall stored magnetic energy of the coil system is 80 GJ. For comparison: The magnetic energy of the SEAFP device is 180 GJ in 16 TF coils and the magnetic energy of the ITER FDR coil system is 120 GJ. Furthermore, the disruption as a major initiator of a quench does not exist in stellarators. A quench is the biggest accident of the coil system for the superconductor, which must be mitigated by a quench detection system and the conversion of the magnetic energy into dump resistors. An upgraded version of the detection system of Wendelstein 7-X has been designed for this purpose [28].

There is no induced toroidal current or a bootstrap current. The design of the magnetic field in the Helias reactor includes zero bootstrap current as one of the design criteria. Such a case will be verified and tested in Wendelstein 7-X. The absence of a toroidal current eliminates the energy reservoir, which can drive tearing modes and disruptive instabilities.

This conclusion also holds for neoclassical tearing modes, which in tokamaks degrade the confinement. In a stellarator without toroidal current only pressure gradient driven MHD-instabilities are possible. Approaching the critical pressure gradient would result in a soft onset of unstable modes and increasing radial plasma losses. There are no experimental or theoretical arguments so far, which predict a violent collapse at the beta limit. In conclusion, any collapse of the plasma energy occurs on the time scale of the energy confinement time, which is on the order of 1.5 s.

13. Conclusions

The magnetic field of the 4–period Helias configuration has been optimised with respect to plasma equilibrium and neoclassical transport, which is extremely low; the effecive helical ripple is below 1%. Fast alpha-particle losses could be reduced to 2.5% of the heating power. Empirical scaling laws (LGS) predict ignition in HSR4/18; an improvement factor is not necessary. However, further theoretical studies are needed to clarify the confinement at the beta-limit, which is expected around 4.3%.

The present engineering studies of a 4-period Helias reactor HSR4/18 have demonstrated the good prospects of this concept as a viable fusion reactor. The configuration HSR4/18 is more compact than the 5-period HSR5/22, which also may lead to a 20% cost reduction of the reactor core. The average neutron wall load will increase to about 1 MW/m^2 at a fusion power of 3000 MW. Therefore the number of maintenance procedures will be smaller than in a more compact tokamak reactor, however the amount of activated waste at shut-down of the reactor will be about the same.

Various blanket concepts developed for tokamak reactors have been studied with respect to their applicability in the Helias reactor. In principle all concepts can be realised in the stellarator reactor, however the three-dimensional geometry requires a large number of different blanket segments, while in axisymmetric devices only two different shapes – inboard and outboard segment – are needed. The blanket segments in the Helias reactor can be replaced through the portholes between adjacent modular coils. Neutronics calculations using the MCNP-code are in preparation, in particular, the effect of the 3-D geometry on the breeding ratio and the activation of the structural material need to be investigated.

Some safety aspects of the stellarator reactor in comparison to a tokamak reactor have been analysed. The absence of current disruptions in stellarators eliminates the risk of destroying plasma-facing components by sudden mechanical loading. Furthermore, a sudden quench of the superconducting coils due to the associated eddy current can be avoided. With respect to nuclear hazards there is no significant difference between stellarators and tokamaks, since at the same fusion power output also the rate of neutron production and consequently all neutron-induced effects are the same.

One major cost-driving item of a fusion reactor is the coil system. Since in HSR4/18 the maximum magnetic field is 10 T, this is still in the range of NbTi technology if cooling at 1.8K can be realised in a reliable way. The total length of superconducting NbTi cable is 400 km and the weight about 807 t. The total weight of the super-conducting coils including the casing is 4430 t. Together with the support system the overall weight will remain below 10000 t, which will keep the costs of the magnet system certainly far below those of an ITER-type tokamak reactor.

References

[1] SAPPER J., RENNER H., Fusion Technology 17 (1990), 62
[2] M. DARWESCHSAD et al. Fusion Technology and Design 45, (1999), 361
[3] BEIDLER, C.D. et al. Proc 16th IAEA Conf. on Fus. Energy, Montreal 1996, IAEA-CN-64/G1-4
[4] HARMEYER, E., et al, Proc. SOFT-21, Madrid 2000, Paper F-44
[5] HARMEYER, E., JAKSIC, N., SIMON-WEIDNER, J, Proc. SOFT-19, Lisboa 1996, Vol. II, p. 1035,
[6] MITCHELL M. Fusion Eng. And Design 46, (1999) 129
[7] STRUMBERGER, E Nuclear Fusion 37 (1997) 19
[8] STRUMBERGER, E., NÜHRENBERG, C. et al., Proc. 26th EPS-Conf. Maastricht, 1999
[9] NÜHRENBERG, C. Phys. Fluids **B5** (1993) 3195
[10] STRUMBERGER, E. et al., IPP-Report IPP III/249
[11] KENDL, A., WOBIG, H., Phys. Plasmas **6**, (1999), 4714
[12] LOTZ W., MERKEL P., NÜHRENBERG J., STRUMBERGER E., Plas. Phys. Control. Fusion 34 (1992) 1037.
[13] WOBIG, H., SIDORENKO, I., SHISHKIN, A.A., IPP-report IPP III/251, Oct. 1999
[14] BÖHME G. et al., IPP-report IPP 2/285, KfK-report KfK 4268, Fusion Power Assoc./Univ. Wisc. FPA-87-2
[15] DALLE-DONNE, M. et al. KfK Report KfK 5429, Nov. 1994
[16] MALANG, S., Limitations on blanket performance, Fus. Eng. and Design **46** (1999) 193
[17] YAMANISHI H et al. *Fus. Eng. Design* 41 (1998) 583
[18] DALLE DONNE M., *European DEMO BOT solid breeder blanket*, KfK-report 5429, (1994)
[19] MALANG S et al. *Development of Self-Cooled Liquid Metal Breeder Blankets*, FZKA 5581, (1995)
[20] WOBIG, H, HARMEYER E, HERRNEGGER F, KISSLINGER J, *Blanket Concepts of the Helias Reactor*, IPP-Report IPP III/244
[21] WOBIG, H. et al. IPP-Report III/244 (1999)
[22] BEIDLER, C.D. et al. Proc 17th IAEA Conf. on Fus. Energy, Yokohama 1998, IAEA-F1-CN-69/FTP/01
[23] GIANNONE, L. et al. Plasma Phys. and Control. Fusion **42** (2000) 603-627
[24] Stellarator Power Plant Study, USSD-ENG-004, (1997)
[25] NADJMABADI F, CONNOR W et al., UCLA-Report UCLA-PPG-1461
[26] BÖHME G at al. IPP-Report 2/285 (1987)
[27] RAEDER J et al. *Report of the SEAFP project* EURFUBRU XII-217/95
[28] WIECZOREK* A. , ZACHARIAS L**, Computer simulations of the power supply and the protection system for the superconducting coils of the fusion reactor (private comm.)